

A high-throughput determination of metal concentrations in whole intact *Arabidopsis thaliana* seeds using synchrotron-based X-ray fluorescence spectroscopy

Lester W. Young,^a Neil D. Westcott,^a Klaus Attenkofer^b and Martin J. T. Reaney^{c*}

^aAgriculture and Agri-Food Canada, 107 Science Place, Saskatoon, SK, Canada S7N 0X2, ^bBESSRC, Advanced Photon Source, Argonne National Laboratory, Building 401, 9700 South Cass Avenue, Argonne, IL 60439, USA, and ^cDepartment of Applied Microbiology and Food Science, 51 Campus Drive, University of Saskatchewan, Saskatoon, SK, Canada S7N 5A8.
E-mail: martin.reaney@usask.ca

The identification of genes involved in metal metabolism in plants requires the 'screening' of thousands of genetic variants. While inductively coupled plasma mass-spectroscopy has been used to identify variants with an altered total metal concentration, a more convenient high-throughput technique capable of examining individual seeds (or other tissues) would be useful. Here, the high brightness of synchrotron radiation has been utilised to examine relative metal concentrations in seeds of the genetically well characterised plant *Arabidopsis thaliana*. The relative concentrations of Mn, Fe, Ni, Cu and Zn in individual seeds were determined using a 500 µm × 500 µm beam. Metal concentrations were normally distributed, except where metal-containing dust contaminated the samples. Neither seed orientation nor genetic background (from three 'wild type' variants with different genetic lineages) had a significant effect on the Zn-normalised metal concentration. No advantages, such as the observation of tissue-specific metal accumulation, were obtained by using a 50 µm × 50 µm beam. A high-throughput proof-of-concept experiment was demonstrated that could be used to screen libraries of genetic variants for individuals with altered metal concentrations. Further work is required to standardise the technique before screening of libraries is possible.

1. Introduction

Numerous genes control metal accumulation in plants (*e.g.* see Delhaize, 1996; Lott & West, 2001; Yoshimura *et al.*, 2000; Lahner *et al.*, 2003); however, few have been identified because the screening of libraries of mutated plants for altered metal concentrations is difficult. Screening requires the analysis of thousands of randomly mutated plants to identify individuals with unusual characteristics and, to date, most techniques for quantifying metals are poorly suited to high-throughput analysis of large populations. In an outstanding example of what may be achieved, Lahner *et al.* (2003) used inductively coupled plasma mass-spectrometry (ICP-MS) to screen 6000 different mutated plants, from which 51 were identified as having altered metal concentrations (Lahner *et al.*, 2003). A technique able to determine metal concentrations *in vivo* with minimal sample preparation would reduce the

amount of work required to obtain these data and likely be much more rapid.

Although ICP-MS is useful for whole-plant determination of metal concentration, quantification of metals in specific tissues and organs would be more useful for identifying genes involved with metal metabolism. We wished to develop a technique capable of determining metal concentrations in individual seeds as opposed to whole plants. Deposition in seed tissues is one of the end points for metals taken up by plants, and perturbations in metal uptake, transport, storage during vegetative growth and final deposition in seeds are likely to alter seed metal content (*e.g.* Delhaize, 1996; Young *et al.*, 2006). A mutation in a gene responsible for metal transport from the leaves to the seeds may be difficult to detect using ICP-MS analysis of a whole plant. Additionally, metal uptake and storage are dynamic in growing plants (Ramesh *et al.*, 2004), whereas in seeds the metal content is assumed to be

stable until germination. Furthermore, seeds are used as both food and feed and therefore identifying genes that affect metal concentrations in seeds has implications in animal and human nutrition.

Ideally, methods for screening mutant libraries for metal concentrations should require little sample preparation and be rapid, sensitive, non-destructive and inexpensive. The method should allow for recovery of the DNA to allow identification of metal metabolism genes. Such a technique will have utility for studying plant metal physiology as well as determining the metal-metabolism gene function.

Germinating seedlings utilize metals as enzyme cofactors and in metabolic processes (for example, establishment and maintenance of membrane potential, cell replication and respiration). High concentrations of different metals, most abundantly magnesium, potassium and calcium, are stored in seeds in preparation for germination (Lott & West, 2001). Relatively lower concentrations of manganese, iron, copper and zinc have also been observed in seeds (Reid *et al.*, 1999; Lott & West, 2001). Seedlings with sufficient accumulations of stored metals have an advantage over intraspecific competitors as more energy can be utilized for growth and metabolism rather than the collection and transport of cations from the environment. Stored metals may also permit cell growth and metabolism in situations where essential elements are lacking in the seedling's immediate surrounds.

Different tissues are expected to have different metal concentrations due to differences in metabolic activity and enzyme composition. For example, Mn can accumulate in mitochondria (Scandalios, 1997) so high concentrations of this metal may occur in tissues with large energy requirements during germination. Higher concentrations of metals may be observed in tissues with high concentrations of metallic enzyme cofactors. For example, higher concentrations of Fe or Mn may be indicative of high superoxide dismutase concentrations (Scandalios, 1997). Tissue-specific differences in *Arabidopsis* seeds have been observed using energy-dispersive X-ray spectroscopy (Lott & West, 2001) and synchrotron-based X-ray fluorescence microprobe (Young *et al.*, 2006).

Collections of *A. thaliana* genetic lines have been developed that include arrays of plants known to contain single mutations in protein coding gene sequences. Three major repositories with single-gene mutated *A. thaliana* seed libraries hold 32500 (as of September 2001), 40000 and 85000 individual lines, at the SALK Institute, Cold Spring Harbour Laboratory and RIKEN Bioresource Center, respectively (Nakazawa *et al.*, 2003; Sundaresan *et al.*, 1995; Martienssen, 1998; Kuromori *et al.*, 2004). The Agriculture and Agri-Food Canada Research Branch has developed its own *A. thaliana* library containing 70000 lines (I. Parkin, personal communication). Examination of these collections using the technique described in this paper will lead to the identification and partial characterization of genes involved in metal metabolism and storage.

In this paper we investigate the use of synchrotron-based X-ray fluorescence (XRF) spectroscopy to examine the relative concentrations of K, Ca, Mn, Fe, Ni, Cu and Zn in intact

Arabidopsis thaliana seeds. Elements from Sc to Cr and Co were below detection limits. XRF has been used to study metal distribution in plants (Pickering *et al.*, 2000; Howe *et al.*, 2003; Yun *et al.*, 1998); however, it has not been utilized to quantify metals in seeds. The high brightness of synchrotron X-ray emissions compared with a conventional source enables a many-fold increase in the rate at which data collection may be performed, as well as a reduction in the size of the observable target objects. In this paper, seeds from the model plant *Arabidopsis thaliana* are used.

A. thaliana offers several advantages for the identification and study of genes involved in metal metabolism, in addition to the vast array of publicly available genetic material mentioned above. The small size of the *A. thaliana* seed makes it uniquely suited to XRF analysis. Attenuation of X-ray fluorescence photons emitted by excited atoms by the seed matter itself is not expected to be a factor in determining metal concentrations, at least for elements heavier than Mn. Estimations of X-ray absorption by cellulose are discussed by McNear *et al.* (2005). The typical size for these oblate-ellipsoid-shaped seeds are 400 μm long by 250 μm at the widest point.

One advantage of using seeds in general is their low water content, which results in lower amounts of radiation damage compared with more hydrated tissues. This means that seeds may be grown after X-ray exposure for easier DNA collection (and gene identification). DNA amplification to identify mutated genes is still possible, using the polymerase chain reaction, from seeds that fail to grow after analysis. Other advantages of using *A. thaliana* include its fast generation time, the relatively small amount of space required to grow the plants and its well characterized genetics.

2. Materials and methods

2.1. Metal concentrations in bulk seed lots

Elemental concentrations in bulked *A. thaliana* seeds were analysed using ICP-MS (Department of Geology, University of Saskatchewan, Saskatoon, SK, Canada) and instrumental neutron activation (INA; ActLabs, Ancaster, ON, Canada). Approximately 100 mg of seed from each of three pot replicates for each ecotype were submitted for analysis.

2.2. Seed growth and sample mounting

Pots of *Arabidopsis thaliana* plants were grown in the AAFC greenhouses using RediEarth without added fertiliser and irrigated using the city water supply. The three ecotypes used were Columbia-4 (Col), Wassilewskija (Ws) and Niederzenz (Nd). All three ecotypes were grown at the same time in adjacent trays to minimize environmental variation. Standard growing conditions were used (16 h/8 h day/night cycle with 295 K/291 K temperatures). Decis and Intercept (both Bayer CropScience) were applied if necessary to control thrips and aphids, respectively. Seeds were harvested from the pots on maturity and desiccated seeds kept at 277 K until use.

Sample-holder windows were made using cardboard frames and adhesive Kapton tape (3M, St Paul, MN, USA) panes. Several different materials and adhesives were examined for suitability as panes, including paper, scotch tape, Teflon tape, plastic cling wrap, static-free plastic, oven-bag plastic, high-density polyethylene, dental adhesive, animal-based paper glue, sucrose-containing paper glue and KY jelly. Most materials had unacceptably high concentrations of the metals of interest and/or functioned poorly in combination with the adhesives tried. Kapton tape provided suitable adhesion of the seeds and low background concentrations of the various elements of interest.

A. thaliana seeds were sprinkled or arranged onto the silicon adhesive of the Kapton tape and the sample windows were mounted onto the sample stage. The sample stage was placed at an angle of 45° to the incident beam and at 45° to the detector. Two actuator motors moved the sample holder in 1 µm steps in the *x* and *y* directions. The *x* direction was at 45° to the incident beam.

Up to 15 seeds were arranged in 5 × 3 grids on the sample holders, spaced 2 mm apart in the horizontal and vertical directions. Four Col grids were made with the seeds on each grid oriented in a similar manner. The grid numbers start at 3 as two test grids were used for technique development. In grids 3 and 4 the seeds were arranged vertically, that is with the root apical meristem and the cotyledon tips pointing to the top of the field of view. The radicles were placed on the right and left for grids 3 and 4, respectively. In grids 5 and 6 the seeds were oriented horizontally, with the radicle on the bottom and pointing to the right and the left of each grid, respectively. Grids 7 and 8 were arrangements of Nd and Ws seeds, respectively. In grid 7, 16 seeds were arranged vertically, the first eight with the radicle on the right, the second eight with the radicle on the left. The Ws seeds in grid 8 were arranged vertically with the radicle on the left.

2.3. Beamline set-up and data collection

Low- and medium-spatial-resolution XRF data were collected using the BESSRC beamline (11-ID-D) at the Argonne National Laboratory, Advanced Photon Source (Beno *et al.*, 2001). Monochromatic X-rays (10 keV) were produced using a 70-pole wiggler insertion device with a 16 cm period and a double-crystal monochromator (Beno *et al.*, 2001). The size of the X-ray beam incident on the sample was controlled by horizontal and vertical slits upstream of the sample. Incident beam intensity was controlled using upstream filters. Low- and medium-resolution pixels were 500 µm × 500 µm and 50 µm × 50 µm in size, respectively. One pixel per seed was used for the low-resolution maps and either 112 or 140 pixels per seed for the medium-resolution maps.

A Vortex silicon drift diode detector (Radiant Detector Technologies, Northridge CA, USA) was placed approximately 1 cm away from the point that the incident beam struck the sample. The detector was oriented perpendicularly in the horizontal plane of the incident beam to minimize exposure to inelastic scattering. A graphical user interface (SPECFE) was

used to both control the beamline optics and to collect the data *via* the programme *SPEC* (Certified Scientific Software, Cambridge, MA, USA). Raw fluorescence data were normalized for variation in the energy of the incident beam (I_0), as measured using an ion chamber.

Raw data for the low-resolution maps were presented both graphically and summarized in table format. Background data points were not taken at this resolution as over half the area of each spot was comprised of background and was assumed to be consistent. Data for the medium-resolution maps were treated as follows for imaging: a threshold mask was determined using the potassium data to identify pixels containing data from the seed; a fifth-order polynomial background wave was calculated for the data outside the threshold mask and subtracted from the normalized data; the subtracted normalized data were interpolated, using a 5 pixel-wide spline function, to create the image maps.

Data manipulation and graphing were performed using *IGOR PRO* (version 5.0.4, Wavemetrics, Lake Oswego, OR, USA). Statistical analyses, except *k*-means clustering, were performed using *SAS* 6.12 (SAS Institute, Cary, NC, USA). *K*-means clustering was performed using the *KMEANS* function in *IGOR PRO* with 1450 points from the XRF spectra (from approximately 230 to 9025 eV) as the dimension data and each pixel a member of the population.

3. Results

3.1. Metal concentrations in bulk and individual seeds using ICP-MS, INA and XRF

The concentrations of metals in the three different *A. thaliana* ecotypes were determined using ICP-MS and INA (Table 1). Some differences in elemental concentration between the ecotypes can be observed; however, the overall pattern of element accumulation remained similar between ecotypes (*e.g.* high concentrations of Mg and Ca and lower concentrations of Mn and Zn). Differences in the ionization of each element during ICP-MS and a range of different technical factors in INA analysis are responsible for the differences in the concentrations recorded between the techniques. The minimum amount of each element detectable by the two techniques was different, but complementary, allowing concentration estimates for all elements of interest to be obtained. These results suggested that the concentrations of several different elements were sufficient for single-seed analysis using XRF.

Synchrotron-based XRF was used to determine the relative concentrations of seven elements (K, Ca, Mn, Fe, Ni, Cu and Zn) in single *A. thaliana* seeds (Table 2 and Fig. 1). Four 5 × 3 grids of *A. thaliana* eco Columbia-4 (Col) seeds were analysed using a 500 µm × 500 µm beam (10 keV). All seeds within a grid (in grids 3-6) were oriented in the same direction and each XRF spectrum was collected for 10 s by the detector. Shapiro-Wilk tests failed to reject the null hypothesis that the data for each grid were not normally distributed, except for five instances. For three of these instances there was a single

Table 1

Concentrations of selected elements determined using ICP-MS and INA in different *A. thaliana* ecotypes.

The concentrations (in ppm \pm standard error) of elements in three 0.1 g replicates of Col, Ws and Nd seed populations were determined. Elements unable to be detected by a technique or at a concentration too low to be consistently determined are indicated with a dash (–).

	Na	Mg	Al	K	Ca	Mn	Fe	Ni	Cu	Zn	Mo
ICP-MS											
Col	–	3340 \pm 175	16.95 \pm 3.31	–	5553 \pm 3	45.37 \pm 1.68	94.72 \pm 2.49	0.57 \pm 0.11	8.84 \pm 0.27	116.1 \pm 14.4	0.42 \pm 0.02
Ws	–	2942 \pm 92	15.10 \pm 5.10	–	5610 \pm 82	74.19 \pm 16.30	96.51 \pm 5.80	0.98 \pm 0.45	9.76 \pm 0.96	113.7 \pm 11.1	0.36 \pm 0.10
Nd	–	2804 \pm 134	13.23 \pm 2.33	–	4808 \pm 444	65.45 \pm 18.11	86.63 \pm 9.61	0.35 \pm 0.03	10.54 \pm 1.58	109.3 \pm 0.2	0.32 \pm 0.06
INA											
Col	147 \pm 4.8	6530 \pm 639	–	29800 \pm 1380	3470 \pm 203	47.0 \pm 6.2	–	–	–	60.0 \pm 6.0	–
Ws	174 \pm 2.1	5930 \pm 617	–	14170 \pm 4249	570 \pm 606	87.2 \pm 6.7	–	–	–	71.7 \pm 5.0	–
Nd	163 \pm 7.5	6270 \pm 696	–	22230 \pm 1795	1370 \pm 949	52.3 \pm 8.5	–	–	–	62.7 \pm 3.8	–

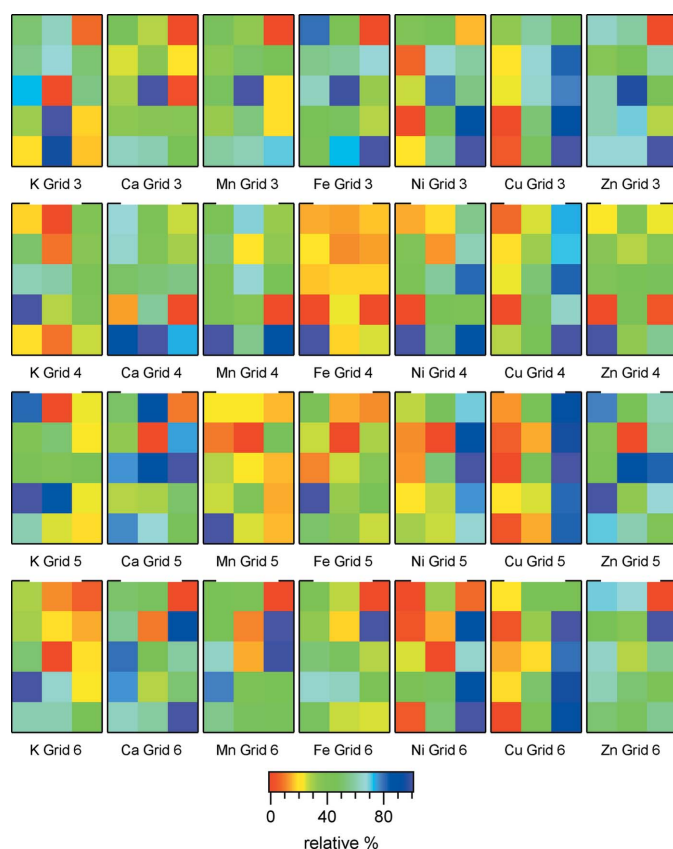


Figure 1

Low-resolution XRF maps of *A. thaliana* eco Col seeds arranged in grids. The seeds for each grid are oriented differently and the relative elemental concentrations shown. Each seed is represented by a single square, the colour of which corresponds to the relative concentration of each element (red = low concentration, relative to the other seeds on the grid).

obvious outlier (Zn in grid 4, seed 1 and Mn and Fe in grid 5, seeds 1 and 2, respectively). When the single outlier was removed and the analysis performed again, the data approached the normal distribution, suggesting that contamination of

the grids with metal-containing particles was responsible for the outliers. Contamination during sample mounting has been shown to occur (Young *et al.*, 2006). The mean and standard deviation for Zn grid 4, Mn grid 5 and Fe grid 5 changed to 1.105 and 0.220, 0.165 and 0.0197 and 0.252 and 0.0288, respectively. No single seed was an obvious candidate for an outlier for either the Fe grid 4 or Cu grid 5 data and as a result the Shapiro–Wilk tests were not re-performed for these data.

The difference in relative elemental concentration, measured using standard deviation/mean, for grids 3–6 ranged from 0.12 to 0.41 (Table 2); that is, one standard deviation was equivalent to 12–41% of the mean value for each element. For all grids and elements the overall standard-deviation:mean ratio was 23%. Assuming that elemental composition is normally distributed, 99% of the population should fall within 2.57 standard deviations of the mean.

Significant differences in XRF intensities between grids were observed for all elements, using a mixed-model analysis in SAS. The total XRF counts between grids were highly significantly different ($p < 0.0001$) from one another. The total XRF for each element was also highly significantly different ($p < 0.0001$), except for Ni ($p \leq 0.1664$). The Ni data are not observed as significantly different from the other elements because the absolute difference between the XRF counts for this element and K and Ca is large. When K and Ca were removed from the analysis, the difference between XRF counts for Mn, Fe, Ni, Cu and Zn was highly significant (not shown).

The highly significant differences in XRF counts between grids are the result of large differences in the absolute values of the data. When the data for each point were normalized, using the Zn XRF value for that data point, the differences between grids was not significant, at $p \leq 0.05$ (Table 3). The ratio of XRF produced by each element does not vary between grids ($p \leq 0.8651$) and, as expected, the amount of each element present is significantly different from each of the other elements ($p \leq 0.0001$; Table 3). A breakdown of this

Table 2

Summary of low-resolution results.

The concentrations of K, Ca, Mn, Fe, Ni, Cu and Zn were determined from single seeds arranged in grids using a single 500 µm × 500 µm X-ray beam. The mean fluorescence produced by each element is indicated ($n = 15$ seeds; except grid 7 where $n = 16$). Shapiro–Wilk tests were performed for each element in each group (W and associated p) to determine if the data approached the normal distribution. An additional test for normality was performed after outliers were removed (bold text). Std = standard deviation. * = single outlier not identified and analysis not reperformed.

Grid	3: Col seeds, vertical with radicles on right							4: Col seeds, vertical with radicles on left						
Element	K	Ca	Mn	Fe	Ni	Cu	Zn	K	Ca	Mn	Fe	Ni	Cu	Zn
Mean	1.686	1.322	0.061	0.111	0.028	0.144	0.369	3.749	3.454	0.222	0.375	0.1397	0.5038	1.170
Std	0.415	0.234	0.012	0.029	0.005	0.030	0.089	1.229	0.765	0.037	0.146	0.017	0.107	0.330
Std/Mean	0.25	0.18	0.20	0.27	0.17	0.21	0.24	0.33	0.22	0.17	0.39	0.12	0.21	0.28
W	0.958	0.923	0.970	0.974	0.978	0.973	0.940	0.933	0.995	0.957	0.572	0.970	0.970	0.871
p	0.654	0.215	0.862	0.910	0.954	0.894	0.382	0.303	1.000	0.643	<0.001	0.860	0.861	0.035
W^\dagger											*			0.918
p^\dagger											*			0.207

Grid	5: Col seeds, horizontal with radicles on bottom and tips pointing right							6: Col seeds, horizontal with radicles on bottom and tips pointing left						
Element	K	Ca	Mn	Fe	Ni	Cu	Zn	K	Ca	Mn	Fe	Ni	Cu	Zn
Mean	3.685	2.945	0.174	0.262	0.087	0.363	0.811	2.193	1.749	0.096	0.167	0.041	0.206	0.509
Std	0.748	0.476	0.039	0.047	0.012	0.089	0.117	0.901	0.499	0.023	0.045	0.006	0.052	0.128
Std/Mean	0.20	0.16	0.23	0.18	0.14	0.24	0.14	0.41	0.28	0.24	0.27	0.15	0.25	0.25
W	0.932	0.959	0.739	0.855	0.942	0.851	0.970	0.932	0.966	0.937	0.945	0.900	0.900	0.952
p	0.290	0.674	0.001	0.021	0.406	0.018	0.865	0.295	0.792	0.346	0.450	0.096	0.097	0.562
W^\dagger			0.959	0.973		*								
p^\dagger			0.702	0.910		*								

Grid	7: Ws seeds, vertically arranged, 8 seeds with radicles on each side							8: Nd seeds, vertically arranged with radicle on left						
Element	K	Ca	Mn	Fe	Ni	Cu	Zn	K	Ca	Mn	Fe	Ni	Cu	Zn
Mean	0.161	0.114	0.007	0.012	0.002	0.016	0.029	2.399	1.949	0.180	0.292	0.071	0.366	0.845
Std	0.064	0.042	0.002	0.005	<0.001	0.004	0.011	0.708	0.652	0.060	0.094	0.013	0.091	0.218
Std/Mean	0.40	0.37	0.32	0.43	0.25	0.28	0.36	0.29	0.33	0.33	0.32	0.19	0.25	0.26
W	0.953	0.955	0.953	0.962	0.975	0.964	0.985	0.885	0.965	0.888	0.934	0.827	0.944	0.966
p	0.535	0.578	0.540	0.697	0.917	0.726	0.991	0.056	0.781	0.062	0.312	0.009	0.435	0.791
W^\dagger												0.929		
p^\dagger												0.291		

† Without outlier.

analysis (Table 3*b*) suggests that most of the differences between total grid XRF intensities were between grid 3 and grid 4 ($p \leq 0.0152$) and grid 3 and grid 5 ($p \leq 0.0311$). The amount of each element present was different from all the other elements analysed ($p \leq 0.0001$). The grid-by-element comparisons showed that the amount of an element on any grid was similar to the amount of the same element on any other grid.

The relative concentrations of metals in Ws and Nd ecotype seeds in a single grid were also analysed (Table 2). The XRF produced approaches normality for both ecotypes, except for single outliers in the Ni and Cu data for Ws seeds. Removal of these outliers meant that the null hypothesis could not be rejected (at $p \leq 0.05$). The intensity of the Nd data was approximately an order of magnitude lower than all the other scans, possibly due to the misplacement of filters in the incident beam. The Zn-normalized concentrations for Mn, Fe, Ni and Cu in the Ws and Nd seeds were not significantly different from those observed in Col (grids 3–6; data not shown). The Zn-normalized values for K and Ca were all significantly different between Col, Ws and Nd seeds, except for Ca grid 3 and Ca grid 5 with Ca grid 7. This result is consistent with the observations made between the Col grids.

3.2. Medium-resolution mapping

The grids used above were mapped at medium resolution to determine whether tissue-specific metal accumulation occurred in seeds (Fig. 2). Some differences in the XRF emitted from each seed were observed at medium resolution; however, individual organs or tissues could not be defined. Up to 140 spectra were recorded per seed, spatially distributed in an array of points, using a 50 µm × 50 µm X-ray beam and 100 µm spacing between points.

The medium-resolution data were not normally distributed using the Shapiro–Wilk test (not shown) as the large number of background pixels skewed the data towards zero. Normality was also not observed when the analysis was repeated using only those pixels located on the seeds due to removal of the low-intensity pixels from the data set. Mean XRF emitted for each element for each seed was calculated from those pixels with a value higher than the background (*i.e.* mean XRF calculated for pixels located on a seed; Table 4). For most elements the mean seed XRF values approached normality, but for some cases this was not the case (Table 4, bold type).

K-means clustering was used to determine whether tissue-specific differences in the spectra of pixels situated within the

body of a seed could be distinguished (Fig. 2c). Pixels in the background and within the body of the seed could be distinguished. Pixels within the seed itself could be distinguished according to approximate location within the body of the seed; that is, at the edge, intermediate and centre of the seed. Differences in tissues, for example between radicles and cotyledons, however, could not be observed. The largest peak in the XRF spectra of pixels located in the background was for argon (approximately 2957 eV), with only a very low level of Cu. In contrast, pixels within the body of the seeds had high levels of K, Ca, Mn, Fe, Ni, Cu and Zn. The height of the peaks in the spectra of pixels located in the edge, intermediate and centre regions increased towards the middle of the seed, suggesting a relationship between XRF emission and sample thickness.

The relationship between XRF produced by the seeds at low and medium resolution were calculated (Table 4, *R*). The mean counts from each pixel located on a seed (*i.e.* excluding background) were calculated and compared with the corresponding low-resolution data. Although the correlation coefficients for some elements in some grids were high (Table 4), no single element or seed orientation provided a better correlation between low- and medium-resolution data.

XRF attenuation was observed for K and Ca but not for the heavier elements. When the ratio of K or Ca to Zn was calculated, the seeds in the resulting intensity map were asymmetric (data not shown). This asymmetry was not observed for the heavier elements, which emitted higher-energy photons. The asymmetric K:Zn and Ca:Zn maps suggest greater absorption of the fluorescent X-rays from the areas of the seed furthest from the detector. X-rays from these distal portions of the seed have a longer path through the seed matter itself and are thus attenuated more than X-rays emitted from atoms closer to the detector.

3.3. Preliminary low-resolution screening technique

To demonstrate the utility of synchrotron XRF for determining relative metal concentrations, 72 Col seeds were arranged in four vertical rows (R1–R4) in a random orientation. The vertical spacing of the seeds was not controlled except that overlaps were minimized. A 100 μm × 600 μm

Table 3
Mixed-model analysis of Zn-normalized XRF counts for Mn, Fe, Ni and Cu from grids 3–6: (a) summary of results; (b) selected differences of least-squared means. This information compares each variable in an effect (*e.g.* grid number or element) with every other variable in the same effect.

Numdf = numerator degrees of freedom. Dendf = denominator degrees of freedom.

(a) Type 3 tests of fixed effects

Effect	Numdf	Dendf	F value	<i>p</i> > <i>F</i>
Grid	3	260	2.41	0.0677
Element	4	259	1650.24	<0.0001
Grid × element	12	259	0.57	0.8651

(b) Selected differences of least-squared means

Effect	Element	Grid	Element	Grid	Estimate	Std Err	df	<i>t</i> value	<i>p</i> > <i>t</i>
Grid		3		4	−0.027	0.011	261	−2.44	0.015
Grid		3		5	−0.024	0.011	259	−2.17	0.031
Grid		3		6	−0.016	0.011	259	−1.50	0.134
Grid		4		5	0.003	0.011	260	0.31	0.760
Grid		4		6	0.011	0.011	261	0.97	0.332
Grid		5		6	0.007	0.011	259	0.68	0.500
Element	Mn		Ni		0.091	0.012	259	7.39	<0.001
Element	Fe		Mn		0.124	0.012	259	10.01	<0.001
Element	Fe		Ni		0.216	0.012	259	17.45	<0.001
Element	Cu		Fe		0.128	0.012	259	10.35	<0.001
Element	Cu		Mn		0.252	0.012	259	20.40	<0.001
Element	Cu		Ni		0.344	0.012	259	27.92	<0.001
Grid × element	Mn	3	Mn	4	−0.030	0.025	259	−1.21	0.229
Grid × element	Mn	3	Mn	5	−0.037	0.025	259	−1.47	0.142
Grid × element	Mn	3	Mn	6	−0.024	0.024	259	−0.97	0.335
Grid × element	Mn	4	Mn	5	−0.007	0.025	259	−0.26	0.794
Grid × element	Mn	4	Mn	6	0.006	0.025	259	0.26	0.797
Grid × element	Mn	5	Mn	6	0.013	0.025	259	0.52	0.601
Grid × element	Fe	3	Fe	4	−0.009	0.025	259	−0.36	0.719
Grid × element	Fe	3	Fe	5	−0.017	0.025	259	−0.69	0.492
Grid × element	Fe	3	Fe	6	−0.034	0.024	259	−1.39	0.166
Grid × element	Fe	4	Fe	5	−0.008	0.025	260	−0.32	0.749
Grid × element	Fe	4	Fe	6	−0.025	0.025	259	−1.00	0.317
Grid × element	Fe	5	Fe	6	−0.017	0.025	259	−0.68	0.500
Grid × element	Ni	3	Ni	4	−0.047	0.025	259	−1.87	0.062
Grid × element	Ni	3	Ni	5	−0.029	0.024	259	−1.19	0.235
Grid × element	Ni	3	Ni	6	−0.007	0.024	259	−0.30	0.765
Grid × element	Ni	4	Ni	5	0.018	0.025	259	0.70	0.483
Grid × element	Ni	4	Ni	6	0.039	0.025	259	1.58	0.116
Grid × element	Ni	5	Ni	6	0.022	0.024	259	0.89	0.373
Grid × element	Cu	3	Cu	4	−0.053	0.025	259	−2.12	0.035
Grid × element	Cu	3	Cu	5	−0.036	0.024	259	−1.49	0.137
Grid × element	Cu	3	Cu	6	−0.017	0.024	259	−0.71	0.480
Grid × element	Cu	4	Cu	5	0.016	0.025	259	0.66	0.510
Grid × element	Cu	4	Cu	6	0.036	0.025	259	1.43	0.154
Grid × element	Cu	5	Cu	6	0.019	0.024	259	0.78	0.434

(height × width) 10 keV beam was used to determine relative metal concentrations in 72 Col seeds arranged in four rows. The sample holder was moved in 100 μm steps in a vertical direction, starting at the bottom of each row, and data collected for 2 s per step. Approximately 95 spectra were obtained from each row with data collection and processing performed as described for the low-resolution mapping. An example of the output is shown in Fig. 3. A total of 72 seeds in four rows were scanned, taking approximately 12 min.

4. Discussion

The accumulation of storage molecules, especially protein, lipid and carbohydrate, in seeds has been characterized fairly

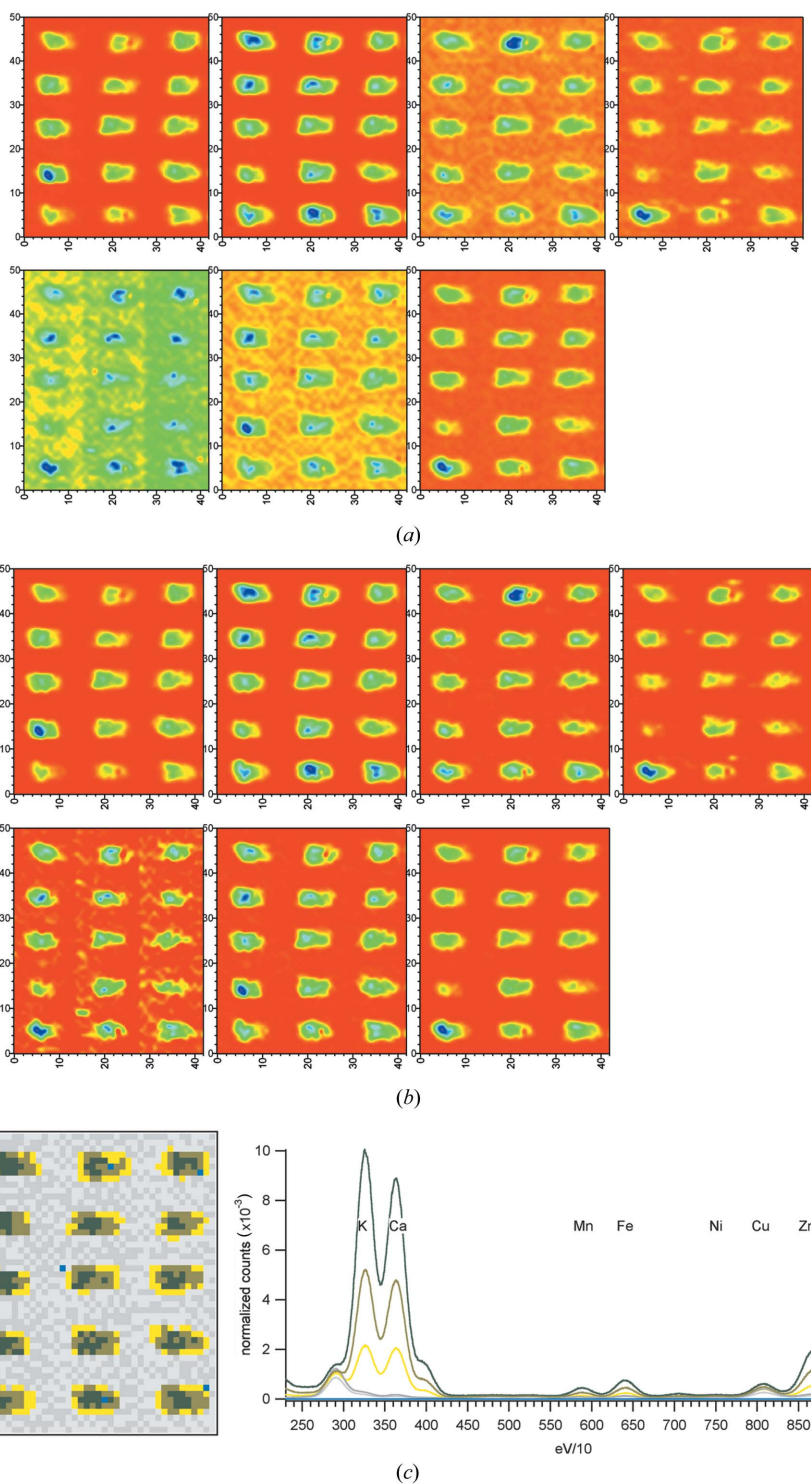


Figure 2 Medium-resolution XRF maps of *A. thaliana* seeds in grid 4. Up to 140 50 $\mu\text{m} \times 50 \mu\text{m}$ points were used to map the metal distribution in each seed. (a) Smoothed data showing, from left to right, K, Ca, Mn Fe, Ni, Cu and Zn distribution. (b) Background-subtracted data showing metal distribution. (c) *K*-means map of grid 4 showing pixels with similar XRF spectra. The graph shows the *k*-means spectra of the coloured pixels in the map.

well (Baud *et al.*, 2002); however, our understanding of metal transport and metabolism in seeds is comparatively less complete. Understanding the accumulation of metals to different tissues will improve our understanding of the processes occurring during germination and will facilitate the

identification and characterization of genes involved in metal accumulation during seed development. A technique able to conveniently survey large numbers of whole tissues or seeds is advantageous to identify metal accumulation mutants. We have demonstrated that synchrotron-based XRF can be used to rapidly determine relative concentrations of Mn, Fe, Ni, Cu and Zn (and other fourth-period elements if present in higher concentrations) in whole *A. thaliana* seeds. The concentrations of K and Ca could also be obtained; however, XRF attenuation by seed tissues limited the usefulness of this technique to quantify relative concentrations of these elements.

The concentrations of the metals examined in this work appear to be normally distributed at the whole seed level. Upper and lower limits for each element will be able to be set so that seeds with an abnormal metal concentration can be detected. These limits are based on the concentration distribution, that is the mean and standard deviation, of each element in the population being studied (Lahner *et al.*, 2003).

The standard deviations for metal concentrations ranged from 12 to 41% of the mean value for each particular element, with an overall mean value of 22%. This compares favourably with the variability observed when using ICP-MS to screen an *A. thaliana* mutant library (Lahner *et al.*, 2003). A better estimate of the variability in elemental concentration will be obtained by analysing a larger number of seeds. The vast majority of the seeds screened using this technique will have a normal concentration of the elements of interest, as genes controlling metal metabolism in these individuals will be fully functional. The mean and standard deviation of the population without a mutation in a metal metabolism gene will approach that of the population as a whole.

Variability between grids was highly significant; however, this was due to the difference in the absolute value of the XRF for each grid. Normalization of the data to the Zn XRF produced by each point showed that there is not a significant difference between the amount of each element present on each grid (Table 3). The reasons for the difference in the absolute amount of XRF

Table 4

Summary of medium-resolution data.

The mean counts per pixel per seed per element per grid, Shapiro–Wilk tests for normality (W and associated p) and the correlation coefficient (R) between mean medium-resolution counts per seed and the corresponding low-resolution value are shown. Data not fitting a normal distribution are highlighted in bold. StdDev = standard deviation.

	K3	Ca3	Mn3	Fe3	Ni3	Cu3	Zn3
Mean	0.196	0.156	0.007	0.014	0.004	0.018	0.043
StdDev	0.044	0.038	0.002	0.005	0.002	0.008	0.014
W	0.977	0.959	0.856	0.828	0.905	0.908	0.893
p	0.941	0.683	0.021	0.009	0.114	0.126	0.074
R	0.403	0.418	0.572	0.738	0.778	0.906	0.771

	K4	Ca4	Mn4	Fe4	Ni4	Cu4	Zn4
Mean	0.347	0.335	0.019	0.033	0.010	0.040	0.098
StdDev	0.086	0.082	0.004	0.012	0.001	0.010	0.025
W	0.861	0.955	0.932	0.730	0.964	0.972	0.911
p	0.025	0.613	0.290	0.001	0.763	0.887	0.141
R	0.934	0.803	0.673	0.933	0.618	0.949	0.899

	K5	Ca5	Mn5	Fe5	Ni5	Cu5	Zn5
Mean	0.278	0.231	0.013	0.019	0.005	0.025	0.059
StdDev	0.047	0.040	0.003	0.004	0.001	0.006	0.010
W	0.973	0.933	0.800	0.940	0.927	0.864	0.974
p	0.904	0.299	0.004	0.387	0.243	0.027	0.915
R	0.927	0.903	0.913	0.808	0.895	0.964	0.864

	K6	Ca6	Mn6	Fe6	Ni6	Cu6	Zn6
Mean	0.152	0.119	0.006	0.010	0.002	0.011	0.031
StdDev	0.047	0.027	0.001	0.002	0.000	0.002	0.005
W	0.953	0.957	0.981	0.967	0.933	0.900	0.877
p	0.580	0.640	0.980	0.820	0.300	0.090	0.040
R	0.921	0.728	0.753	0.606	0.301	0.837	0.746

	K7	Ca7	Mn7	Fe7	Ni7	Cu7	Zn7
Mean	0.424	0.302	0.024	0.042	0.012	0.058	0.111
StdDev	0.093	0.064	0.003	0.007	0.002	0.012	0.013
W	0.968	0.989	0.901	0.959	0.959	0.968	0.941
p	0.811	0.999	0.084	0.651	0.644	0.809	0.362
R	0.535	0.620	0.195	0.518	0.798	0.883	0.565

	K8	Ca8	Mn8	Fe8	Ni8	Cu8	Zn8
Mean	0.267	0.212	0.017	0.027	0.006	0.034	0.075
StdDev	0.053	0.056	0.005	0.006	0.001	0.008	0.013
W	0.883	0.954	0.822	0.936	0.944	0.938	0.909
p	0.052	0.585	0.007	0.340	0.430	0.359	0.131
R	0.409	0.712	0.815	0.690	0.541	0.887	0.651

from each grid are not known. Differences in beam intensity over time could be a possible cause of variability; however, this factor was taken into account by normalizing all data by the ion chamber values, I_0 . Seed orientation is not thought to have caused the difference in absolute XRF counts, as the grids with seeds aligned in the same manner, *i.e.* grid 3 with grid 4 and grid 5 with grid 6, did not have similar intensities (see Table 2).

Other orientation-specific differences between the grids could include the area of the seed cross section exposed to the beam, orientation-specific X-ray attenuation or tissue-specific metal accumulation, although all seem unlikely

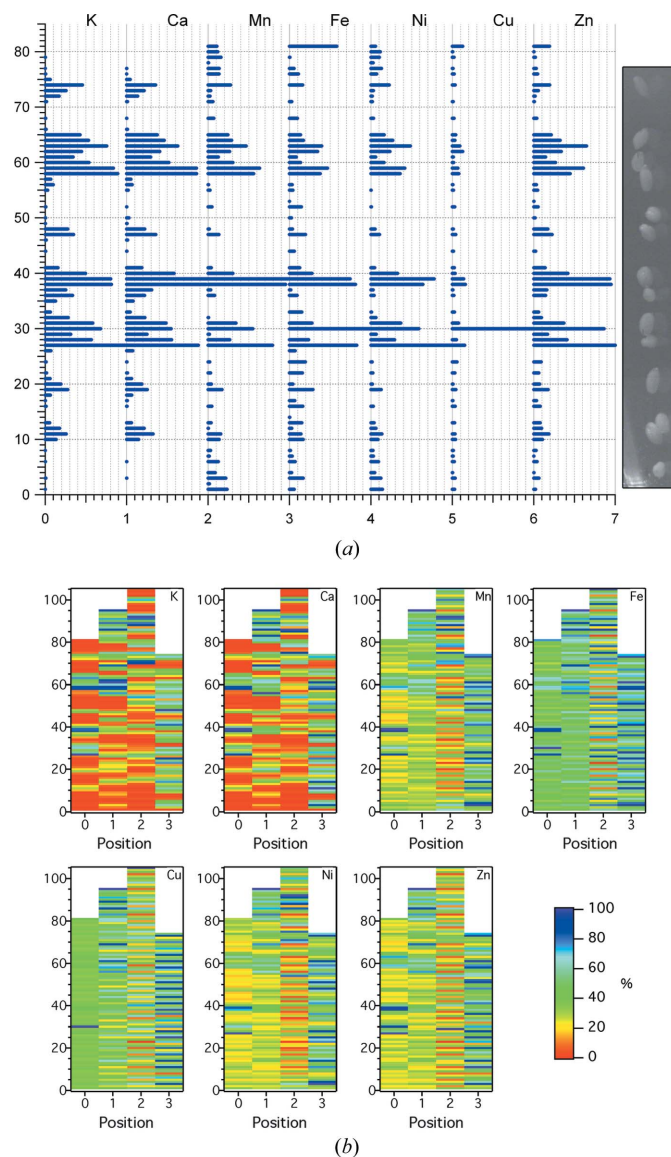


Figure 3
Preliminary seed-screening results. (a) Examples of the results obtained from one row of seeds [position 0 in (b) shown]. (b) Relative concentrations of each element from four rows of seeds ($n = 72$; positions 0–3) from one array. The y axis shows the number of data points and corresponds to 100 μm steps of the beam.

factors. If seed cross sections exposed to the beam caused differences in XRF intensity, we would expect grid 3 to be more similar to grid 4 and grid 5 in the same group as grid 6, something that was not seen. XRF attenuation was only observed for K and Ca and not with the heavier elements (this study, and Young *et al.*, 2006). Tissue-specific metal accumulation has been observed using a 10 $\mu\text{m} \times 10 \mu\text{m}$ microprobe beam (Young *et al.*, 2006); however, the only observable differences in the medium-resolution data were due to the apparent thickness of the seeds. Spatial differences may have resulted from differences in the cardboard windows used to hold the Kapton tape frames.

Using an internal standard may be one way of reducing variability. Normalizing with the Zn data will not be acceptable in the long run due to the normal variability in the

concentration of this element and the loss of information identifying genes involved with Zn metabolism. Zn was chosen as the normalizing element as it is an essential enzyme cofactor and it emits high-energy X-rays that are not attenuated significantly by the seed matter. Feeding the plants with an element found only in low concentrations, such as Ti, Cr, Co or Se, is a possibility; however, a number of uncertainties, such as uptake and toxicity and biological variability, become factors determining the concentration of the internal standard in the plant. Another possibility is to coat the seeds with a salt solution at a known concentration; however, this technique assumes that the surface area and adsorption of the solution is constant across the population, which is unlikely. Finally, a known volume of a standard solution, such as potassium permanganate, could be placed on a spot in lieu of a seed and used as a standard for each grid. The use of a coloured substance such as potassium permanganate has the additional advantage that the colour intensity of each spot could also be measured and the concentration calibrated.

To gain a better understanding of inter-grid variability, multiple time-differentiated analyses of the same grid should be performed. Data on the effects of different orientation on XRF will be obtained by rotating a single grid around the axis of the beam so that the same seeds are analysed from different orientations. Finally, a mechanical means of placing seeds in grids so that the same seed orientation is maintained should be devised. The window material should be less flexible than the cardboard used for this experiment in order to reduce possible spatial changes.

The screening technique described in this paper still requires some development before it can be used for routine screening of *A. thaliana* seeds or other tissues. Seed placement and orientation within the rows must be simplified and made more consistent to aid automation of data collection. Additionally, consistent seed orientation may help reduce some of the variability. A better indication of the variability in elemental concentrations between seeds will be obtained by sampling a larger number of seeds. Finally, oversampling may reduce signal variability resulting from tissue-specific (or non-homogeneous) metal accumulation within the seeds. That is, moving the $100\ \mu\text{m} \times 600\ \mu\text{m}$ beam in $33\ \mu\text{m}$ increments (instead of $100\ \mu\text{m}$) and calculating a weighted average for each point.

A. thaliana seeds were chosen for four reasons. First, they have been completely sequenced and a library of seeds each with a single gene mutated is available. This library will be our starting material for future screens. Second, any genes identified as having an effect on metal accumulation in seeds will be compared with those previously identified as having a role in metal metabolism in whole plants (Lahner *et al.*, 2003; Delhaize, 1996). The suite of genes controlling metal concentrations in whole plants will be similar, but not entirely contiguous, with the set affecting accumulation in seeds. This information will be useful for identifying gene function and characterizing tissue-specific expression patterns. Third, the small size of *A. thaliana* seeds means that the effects of X-ray attenuation may be avoided for the study of elements from Mn

and heavier. Fourth, we have developed a technique to map elemental distribution in *A. thaliana* seeds using XRF (Young *et al.*, 2006). This mapping technique will be useful for characterizing the phenotype of seeds (and other tissues) from plants with metal-metabolism mutations.

One limitation with XRF is attenuation of the low-energy X-rays emitted by the lower-atomic-weight elements. We observed attenuation of the K and Ca signals in the medium-resolution data. XRF microprobe mapping of elements in *A. thaliana* seeds also showed attenuation of the K and Ca signals (Young *et al.*, 2006). Quantification of the lower-atomic-mass elements (lighter than Ca) may be problematic for this reason. X-ray attenuation through thicker tissues may also limit the utility of the medium-spatial-resolution mapping technique, especially in larger tissues. The thickness of the sample being analysed is dependent on the energy of the photons emitted from the metal being examined. Attenuation of the K and Ca signals was more apparent in high-resolution mapping ($8\ \mu\text{m} \times 8\ \mu\text{m}$ pixels), discussed elsewhere (Young *et al.*, 2006). Using X-ray absorption rather than fluorescence may be a better technique for determining metal distribution and/or concentrations when lower-atomic-number elements or thicker samples are being examined.

Another difficulty identified in the low-resolution data was the presence of what were assumed to be contaminating particles. Pixels with abnormally high XRF intensities were detected as the data did not fit the expected normal distribution. In a screening test, this could potentially lead to a false-positive result for that seed. The grids in this experiment were prepared at the beamline and the contaminants were probably incorporated during sample mounting. Sample contamination could be reduced by mounting the samples in a low-dust environment away from the beamline. The number of false positives will be reduced during a screening experiment as a large number of seeds will be examined (at least 3000 individual lines). A good estimate of the mean XRF intensity and variability will thus be achieved, increasing confidence when identifying seeds with abnormal metal concentrations. In addition, more than one seed per line will be analysed, to account for biological variability. Examining multiple individuals from the same genetic line will reduce the chances of false positives from occurring. Finally, all lines identified with abnormal metal concentrations will be propagated after identification using identical growth-chamber conditions and metal content examined again to take environmental variability into account. False positives will be identified at this stage.

The advantage of using synchrotron-based XRF to determine metal concentrations is that short data-collection times may be possible when using small spot sizes. Short data-collection times make the technique amenable for high-throughput screening. This is especially attractive for researchers in the genomics area, as identifying genes involved in metal metabolism requires the analysis of thousands of genetic mutants. While the small size of *A. thaliana* seeds reduces the amount of signal attenuation, a small incident-beam spot size is required for mapping and low absolute

amounts of the elements of interest are present. The high brilliance of synchrotron light produces sufficient signal to allow low concentrations of metals to be detected using small beam areas in a reasonable amount of time. Such analyses are not possible using conventional X-ray sources. For example, 50 μm \times 50 μm beam sizes and 10 s collection times are possible at many beamlines.

One other advantage of using XRF is that it does not physically destroy the sample. Future work will determine whether seeds exposed to synchrotron radiation are still able to germinate (and be propagated). The germination and growth of individual plants that have been analysed directly using this technique will ease the identification of genes involved with metal metabolism. If exposure to synchrotron radiation proves to be inimical to germination, then polymerase chain reaction amplification of the mutated genes from a seed will be technically simple (for example, see Lin *et al.*, 1999).

Drawbacks of using synchrotron-based XRF screening of plant libraries include the high cost and low availability of beam time and the need to develop a consistent seed-mounting method that avoids sample contamination.

Financial support for this project was supplied by Genome Prairie's 'Enhancing Canola Through Genomics' project with travel support from the Saskatchewan Synchrotron Institute. Thanks to Rory Degenhardt for help with the statistical analysis.

References

- Baud, S., Boutin, J.-P., Miquel, M., Lepiniec, L. & Rochat, C. (2002). *Plant Physiol. Biochem.* **40**, 151–160.
- Beno, M. A., Kurtz, C., Munkholm, A., Rutt, U., Engbretson, M., Jennings, G., Linton, J., Knapp, G. S. & Montano, P. A. (2001). *Nucl. Instrum. Methods Phys. Res. A*, **467–468**, 694–698.
- Delhaize, E. (1996). *Plant Physiol.* **111**, 849–855.
- Howe, J. A., Loeppert, R. H., DeRose, V. J., Hunter, D. B. & Bertsch, P. M. (2003). *Environ. Sci. Technol.* **37**, 4091–4097.
- Kuromori, T., Hirayama, T., Kiyosue, Y., Takabe, H., Mizukado, S., Sakurai, T., Akiyama, K., Kamiya, A., Ito, T. & Shinozaki, K. (2004). *Plant J.* **37**, 897–905.
- Lahner, B., Gong, J., Mahmoudian, M., Smith, E. L., Abid, K. B., Rogers, E. E., Guerinot, M. L., Harper, J. F., Ward, J. M., McIntyre, L., Schroeder, J. I. & Salt, D. E. (2003). *Nat. Biotech.* **21**, 1215–1221.
- Lin, Y., Sun, L., Nguyen, L. V., Rachubinski, R. A. & Goodman, H. M. (1999). *Science*, **284**, 328–330.
- Lott, J. N. A. & West, M. M. (2001). *Can. J. Bot.* **79**, 1292–1296.
- McNear, D. H., Peltier, E., Everhart, J., Chaney, R. L., Sutton, S., Newville, M., Rivers, M. & Sparks, D. L. (2005). *Environ. Sci. Technol.* **39**, 2210–2218.
- Martienssen, R. A. (1998). *Proc. Natl. Acad. Sci. USA*, **95**, 2021–2026.
- Nakazawa, M., Ichikawa, T., Ishikawa, A., Kobayashi, H., Tsuhara, Y., Kawashima, M., Suzuki, K., Muto, S. & Matsui, M. (2003). *Plant J.* **34**, 741–750.
- Pickering, I. J., Prince, R. C., Salt, D. E. & George, G. N. (2000). *Proc. Natl. Acad. Sci. USA*, **97**, 10717–10722.
- Ramesh, S. A., Choimes, S. & Schachtman, D. P. (2004). *Plant Mol. Biol.* **54**, 373–385.
- Reid, D. A., Lott, J. N. A., Attrech, S. M. & Fowke, L. C. (1999). *Plant Sci.* **141**, 19–27.
- Scandalios, J. G. (1997). *Molecular Genetics of Superoxide Dismutases in Plants, Oxidative Stress and the Molecular Biology of Antioxidant Defences*, edited by J. G. Scandalios, p. 527. Plainview, NY: Cold Spring Harbour Laboratory Press.
- Sundaresan, V., Springer, P., Volpe, T., Haward, S., Jones, J., Dean, C., Ma, H. & Martienssen, R. (1995). *Genes Dev.* **9**, 1797–1810.
- Yoshimura, E., Sakaguchi, T., Nakanishi, H., Nishizawa, N. K., Nakai, I. & Mori, S. (2000). *Phytochem. Anal.* **11**, 160–162.
- Young, L., Westcott, N., Christensen, C., Terry, J., Lydiate, D. & Reaney, M. (2006). Submitted.
- Yun, W., Pratt, S. T., Miller, R. M., Cai, Z., Hunter, D. B., Jarstfer, A. G., Kemner, K. M., Lai, B., Lee, H.-R., Legnini, D. G., Rodrigues, W. & Smith, C. I. (1998). *J. Synchrotron Rad.* **5**, 1390–1395.